REMARKS

Amendments

New claims 38-45 are directed to further aspects of applicants' invention. Support for these claims can be found throughout the disclosure. See, e.g., the examples of contrast agents described in the specification such as iotrolan, a monomeric, iodine-containing, non-ionic contrast agent, and a iopromide, a dimeric, iodine-containing, non-ionic contrast agent. See, e.g., page 6, lines 17-22 and the agents used in Examples 1 and 2.

Rejection of Claims 1-17 Under 35 U.S.C. §103

Claims 18-38 were rejected as being obvious in view of Nitecki et al. in combination with Chang et al., Ranney, Brash et al., Hilger et al., Kirpoitin et al., and Platzek et al. This rejection is respectfully traversed.

This rejection focuses on the disclosure in Nitecki et al. at column 2, lines 31-353 regarding the possible use of contrast media, capable of marking the vascular space, in mammography. Particularly, the disclosure of Nitecki et al. concerns iodine-containing peptides. Nitecki et al. does not suggest that all contrast agents could possibly be used in mammography nor does Nitecki et al. suggest that any contrast agents is suitable for the low levels of radiation used in projection mammography.

Applicants' claimed method is directed to projection mammography. As described in the specification, low radiation is commonly used in projection mammography. See, e.g., the bottom of page 5 and the middle of page 6.

Enclosed is a copy of Fritz et al., "Scatter/Primary Rates for X-Ray Spectra Modified to Enhance Iodine Contrast in Screen-Film Mammography," Med. Phys. 10(6), Nov/Dec (1983), pp. 866-870. In the Introduction, the authors state:

> Investigation of the use of computed tomography (CT) in breast cancer detection has shown that concentration of iodine-containing contrast material by breast cancer is a very useful diagnostic sign. However, the use of CT body scanners requires rather high tissue doses compared with mammography and entails more expense and time. We are currently investigating the use of modified spectra in a mammographic imaging system to enhance the tissue-iodine contrast for detection of contrast material uptake.

Thereafter, at the end of the Discussion the authors conclude:

> At the current state of development, the cerium anode x-ray tube is limited to fluoroscopic techniques only. For conventional mammographic imaging, this might be adequate due to higher penetration of these photons. However, for contrast mammography the dual requirements of heavy filtration and scatter removal make the cerium anode tube inadequate for clinical imaging. New developments in anode construction and materials will be required to make it useful. The W/Ce system, however, has excellent promise as a tool for observing low-contrast iodine concentrations seen in work with the CT/M.

Thus, at that time, no adequate method existed. The proposed W/Ce system has not been shown to remedy the problem. For example, see the comprehensive review article by Newstead et al. from 1995 (Radiographics, Vol. 15, No. 4, pp. 951-962, July 1995). This article does not mention contrast enhancement in x-ray mammography.

It is respectfully submitted that the rejection fails to set forth sufficient motivation to modify the prior art disclosures so as to arrive at an embodiment in accordance with applicants' claimed method of projection mammography. Withdrawal of the rejection under 35 U.S.C. §103 is respectfully requested.

Respectfully submitted,

Brion P. Heaney (Reg. No. 32,542)
Attorney for Applicant(s)
MILLEN, WHITE, ZELANO & BRANIGAN, P.C.
Arlington Courthouse Plaza I, Suite 1400
2200 Clarendon Boulevard
Arlington, Virginia 22201
(703) 812-5308 [Direct Dial]
(703) 243-6410 [Facsimile]
Internet Address: heaney@mwzb.com

Filed: **October 30, 2001**

BPH:imm\K:\Sch\1653\Preliminary Amend for CPA.wpd

VERSION WITH MARKINGS TO SHOW CHANGES MADE

IN THE CLAIMS:

Please add the following new claims:

-- **38.** A method of projection mammography according to claim 19, wherein said intravenous contrast agent is a non-polymer iodine containing agent.

39. A method of projection mammography according to claim 19, wherein said intravenous contrast agent is a non-peptide iodine-containing agent.

40. A method of projection mammography according to claim 19, wherein said intravenous contrast agent is a monomeric non-ionic iodine-containing agent.

41. A method of projection mammography according to claim 19, wherein said intravenous contrast agent is a dimeric non-ionic iodine-containing agent.

42. A method of projection mammography according to claim 37, wherein said intravenous contrast agent is iopromide or iotrolan.

43. A method of projection mammography according to claim 21, wherein said intravenous contrast agent is N-cetyl-N,N,N-triethylammonium bromide.

44. A method of projection mammography according to claim 22, wherein said intravenous contrast agent contains a compound of an element of atomic number 83.

45. A method of projection mammography according to claim 23, wherein said chelate is (4S)-4-(ethoxybenzyl)-3,6,9-tris(carboxyatomethyl)-3,6,9-triazaundecanoic acid. --

Scatter/primary ratios for x-ray spectra modifi d to enhance iodine contrast in screen–film mammography

Steven L. Fritz, C. H. J. Chang, and William H. Livingston

Department of Diagnostic Radiology, University of Kansas, College of Health Sciences and Hospital, Kansas City, Kansas 66103

(Received 11 August 1982; accepted for publication 26 July 1983)

Contrast mammography to detect the uptake of iodine-containing contrast material may be enhanced by spectral modification of the x-ray beam. Luminance scatter-to-primary ratios were measured for three candidate x-ray tube anode/filter combinations (Mo/Mo, W/Ce, and Ce/Ce). Results show that scattered radiation is significant for all tubes, is lowest for the Mo/Mo system and is essentially the same for the tungsten and cerium anode systems.

Key words: mammography, *K*-edge imaging, contrast materials, x-ray tubes, scattered radiation

INTRODUCTION

Investigation of the use of computed tomography (CT) in breast cancer detection has shown that concentration of iodine-containing contrast material by breast cancer is a very useful diagnostic sign.[1] However, the use of CT body scanners requires rather high tissue doses compared with mammography and entails more expense and time. We are currently investigating the use of modified spectra in a mammographic imaging system to enhance the tissue-iodine contrast for detection of contrast material uptake.

The concept of increasing the radiographic contrast of iodine in the body by x-ray spectral modification and subtraction has been extensively investigated in recent years.[2–5] Typically, spectral modification is achieved by selective filtration of a bremsstrahlung spectrum to achieve a "quasi-monoenergetic" spectrum with a mean energy close to the *K* edge of iodine (33.1 keV).

Cerium, with a *K* edge at 40.45 keV, provides a reasonable balance between transmission of sufficient x-ray intensity to be useful and proximity to the *K* edge of iodine. The use of cerium as a filtration material has been extensively investigated by Kelcz, Mistretta, Kruger, and Riederer.[2–4]

This very attractive idea represents a complex compromise involving x-ray tube heat loading, differential transmission above and below the *K* edge of the filter, patient thickness, resolution, contrast, noise, and scatter. Optimization of the x-ray filter requires reasonably precise knowledge of these imaging characteristics.

This paper presents the results of luminance scattered radiation measurements on two quasi-monoenergetic x-ray spectra being considered for contrast mammography and a conventional screen–film mammographic spectrum. The resultant measurements are compared with previously published data on scatter in mammography and the impact of scatter in mammographic imaging is discussed.

METHODS

The three x-ray anode/filtration combinations used were Mo/Mo, Ce/Ce, and W/Ce. Source characteristics are summarized in Table I. All x-ray measurements were made by exposing a vacuum bagged mammographic screen–film system (Kodak Min R/Ortho M) mounted on an optical bench system. The W and Ce anode tubes were powered by a Siemens Tridoros generator operating in the fluoro mode. The Mo/Mo source was powered by a CGR Senographe generator, operating generally at 10 to 20 mA. All exposures were done at 7.7 s. The W/Ce and Ce/Ce sources were both powered by a Siemens Tridoros generator operating in the fluoro mode. All exposures with either of these two systems were done at 2 or 3 mA and a 300-s exposure time. This was necessitated by the very low output of the Ce/Ce and W/Ce sources as indicated in Table I. Spectra from which the beam characteristics were calculated in Table I were taken with Canberra planar HpGe detector (Model 7110010) and a Canberra Series 80 MCA.

Sensitometry was performed on an x-ray optical bench. For various focus–film distance (FFD) values from 40 to 220 cm, exposures were made to a set of small areas on a single sheet of film. Two sensitometric curves were constructed. One for the Mo/Mo source was done using that source and a 7.7-s exposure time. A second curve for the W/Ce and Ce/Ce sources was made using the Ce/Ce source and a 300-s exposure time. Optical density measurements in the exposed areas were made with a Tobias TBX point densitometer. Corresponding x-ray intensities were measured with a Keithley 96035 ionization chamber and a Keithley 602 electrometer. Relative intensities were also computed using the inverse square law and attenuation of the measured output spectrum by air. Both measurements gave virtually identical values. The resulting curves of log exposure versus optical density were plotted on an absolute exposure scale for 7.7-

 0094-2405/83/060866-05$01.20

TABLE I. Characteristics of three contrast mammography x-ray sources.

Model	Anode	Filtration	kVp	Max mA	Max output (R/s)[b]	Average energy: Incident spectrum	Average energy: Attenuated by 5 g/cm² Lucite
CGR Senographe	Mo	30 mg/cm² Mo	30	40	2.39×10^{-1}	18.2	20.5
Eimac	W	340 mg/cm² Ce	55	4	2.2×10^{-4}	35.5	35.8
Machlett Dynamax M-64[a]	Ce	340 mg/cm² Ce	55	~3	3.06×10^{-4}	35.8	36.0

[a]Specially constructed with cerium film on a molybdenum anode for this project.
[b]Output measured at 1 m FFD for kVp indicated at max mA.

and 300-s exposures to observe the effect of reciprocity failure. From this sensitometric data, experimental log exposure values were computed by semilog interpolation. The 7.7-s curve was used for all exposures with the Mo/Mo system and the 300-s curve was used for both Ce/Ce and W/Ce exposures.

The approach to luminance scatter measurement which was used is illustrated in Fig. 1. A small lead disk (A) was centered in a 5-, 10-, or 15-cm-diam field at the surface of a variable thickness polyethylene phantom (B). The density of the polyethylene was 1.0 g/cm³. Images were obtained for disk diameters of 14, 7, and 5 mm with a mammographic rare earth screen–film system (Kodak Min R/Ortho M) in direct contact (C) with the phantom (B). For each film, the optical density was measured beneath the lead disk and at four points outside the disk in close proximity. From these optical density measurements and the sensitometric data, the primary and scatter components of screen luminescence were calculated. Extrapolation of the scatter/primary (S/P) ratio to zero disk size was used to arrive at a value of S/P for the selected field size and thickness.

RESULTS

Sensitometric curves for 7.7- and 300-s exposure times are shown in Fig. 2. Also shown in Fig. 2, at an arbitrary point on the log exposure scale, is a simulated sensitometric curve supplied by Kodak for a 0.5-s exposure. There are small differences in the shape of the curve at various exposure times, and substantial differences in speed for the two measured curves, due to reciprocity failure.

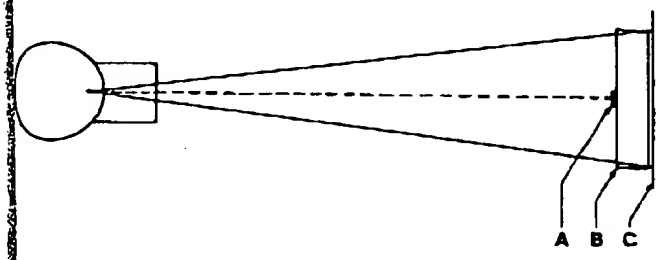

FIG. 1. Experimental geometry for scatter measurement. Consists of collimated x-ray tube, beam blocker (A), scattering phantom (B), and screen/film system (C).

Luminance scatter/primary ratios are shown in Figs. 3–5 for the three sources examined and the three different field sizes tested. Phantom thicknesses are shown as the product of material density and thickness to facility the comparison with other published values. Figure 3 also includes data from Barnes and Brezovich[6] for scatter from a Mo/Mo system at 32 kVp and 14-cm field diameter. The S/P values measured in this study are somewhat higher than those observed by Barnes and Brezovich, and a representative value of the discrepancy is illustrated in Table II along with S/P values for the cerium filtered systems at the same phantom thickness. Both Ce/Ce and W/Ce systems exhibit substantially higher S/P values than the traditional mammographic systems.

In all systems examined, the data were consistent with previous findings[7] that luminance scatter/primary ratio in-

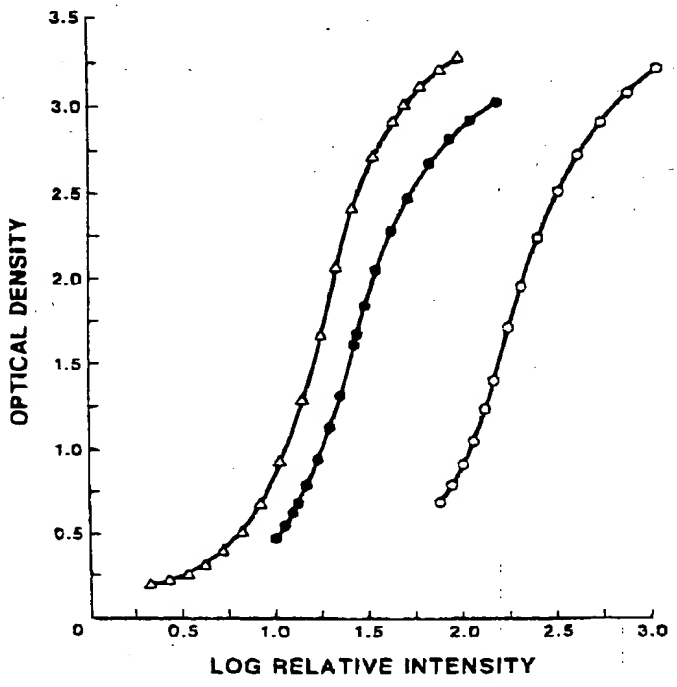

FIG. 2. Sensitometric curves for Kodak Min-R screen with Kodak Ortho-M film. Data for 0.5-s exposure time (Δ–Δ) was supplied by Kodak from simulation studies. Experimental data was taken for this report for exposure times of 7.7 (●–●) and 300 s (○–○).

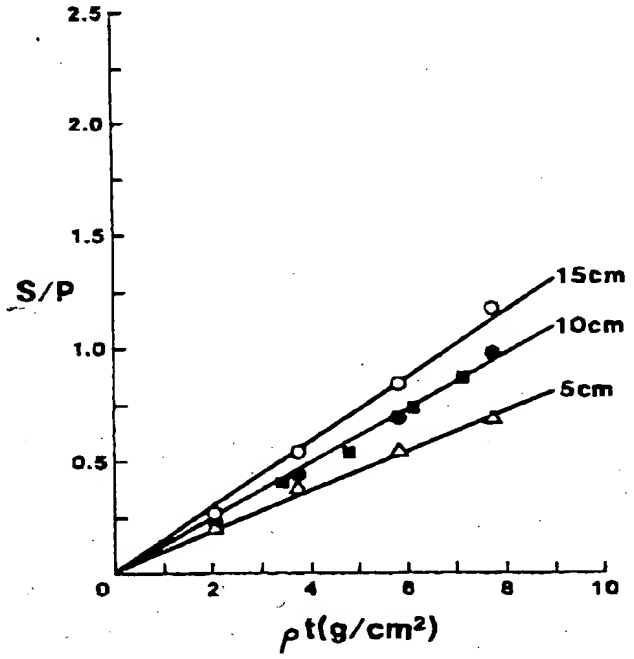

FIG. 3. S/P ratios for the Mo/Mo system at 30 kVp. O–O 15-cm field diameter; ●–● 10-cm field diameter; Δ–Δ 5-cm field diameter; ■–■ 14-cm field diameter [Barnes and Brezovich (Ref. 6)].

creases linearly with absorber thickness, and for a constant thickness plateaus with increasing field size.

DISCUSSION

The intensity of scattered radiation has long been known to be significant even at mammographic energies. Luminance scatter intensities observed in this study are somewhat higher than those observed by previous researchers,[6–12] whose work was summarized by Barnes.[7] In particular, at 5.95 g/cm² Barnes and Brezovich[6] observed $S/P = 0.71$ for a 14-cm field diameter. Interpolation in Fig. 3 gives a value of $S/P = 0.83$ for a 6 g/cm² polyethylene phantom. Since polyethylene has ~8% higher electron density than polymethylmethacrylate (Lucite) used by Barnes and Brezovich and since the difference in field sizes accounts for a small difference in S/P, this discrepancy is not considered significant.

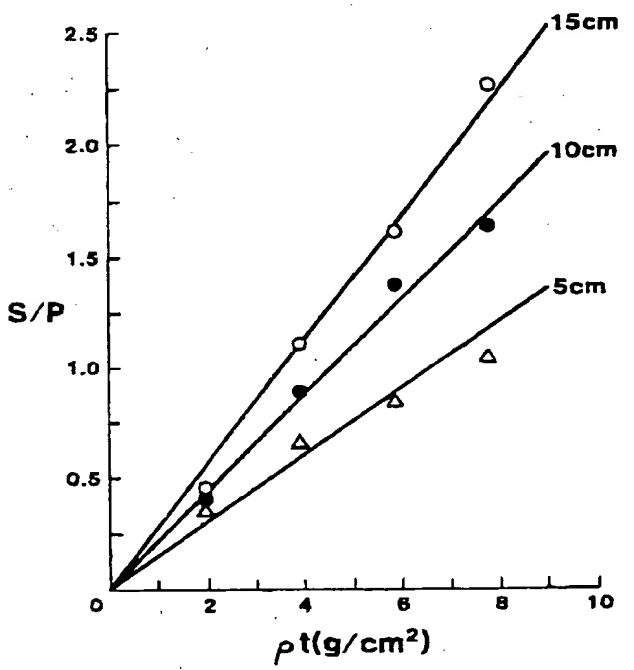

FIG. 4. S/P ratios for the W/Ce system at 55 kVp. O–O 15-cm field diameter; ●– 10-cm field diameter; Δ–Δ 5-cm field diameter.

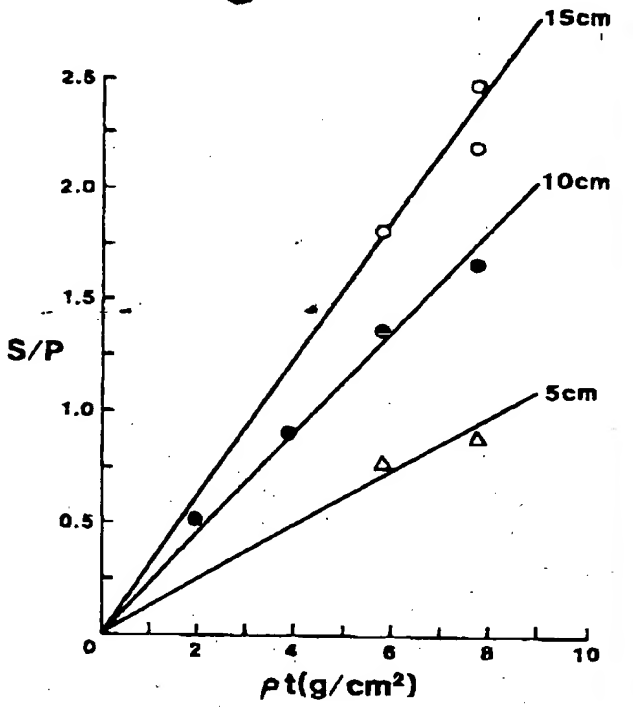

FIG. 5. S/P ratios for Ce/Ce system at 30 kVp. O–O 15-cm diameter; ●–● 10-cm field diameter; Δ–Δ 5-cm field diameter.

At the higher average energies of the Ce/Ce and W/Ce spectra, S/P was considerably higher than for the Mo/Mo spectrum. It is conventional wisdom that scatter/primary fluence ratios increase with increasing energy throughout the diagnostic energy region, particularly at low kVp values. Yet Kalender[13] has shown that even though scatter/primary ratio measured by screen–film sensitometry may rise with increasing energy, the scatter/primary fluence ratio may remain constant or even decline slightly. This is due to the fact that the difference in energy between scattered and primary photons, and therefore the difference in absorption efficiency, increases with increasing energy. Thus it becomes important to distinguish between luminance scatter/primary ratios, as measured in this work, and fluence scatter/primary ratios, as measured, e.g., by Dick *et al.*[14]

It is not clear what the relationship is between scatter and primary x-ray fluence below 30 keV. It may increase with increasing energy[13] or remain constant.[14] However, the data are in agreement that recorded S/P at these energies for screen–film imaging systems increases with increasing energy. Thus scatter will degrade image quality more for quasi-

TABLE II. S/P ratios for three contrast mammography systems.

System	kVp	Reference	Phantom	Field diameter (cm)	Thickness (g/cm²)	S/P
Mo/Mo	32	Barnes and Brezovich[a]	Lucite	14	5.95	0.71
	30	Present work	Polyethylene	15	6.0	0.83
Ce/Ce	55	Present work	Polyethylene	15	6.0	1.8
W/Ce	55	Present work	Polyethylene	15	6.0	1.8

[a]Reference 16.

monoenergetic spectra than for conventional film mammography sources.

In the Appendix, it is shown that for quantum mottle-limited systems, the minimum observable contrast will rise linearly as $\sqrt{1+(S/P)}$. Dose must rise in proportion to $[1+(S/P)]$ to maintain a constant signal-to-noise ratio (SNR). For subtraction imaging, a common tool for observing minimal amounts of contrast material, the SNR degradation is worse. In subtraction imaging, the quantum mottle associated with scattered radiation remains in the subtracted image even though the average intensity of scattered radiation may cancel. This requires a higher dose for a subtraction image than for a nonsubtracted image with the same SNR.

Fortunately, image quality may be improved substantially by removing scattered radiation. Grids accomplish this at the cost of increased dose. Barnes *et al.*[15] have shown that scatter can be reduced to very low levels in mammographic imaging through the use of a scanning multiple-slit assembly. The advantage of this approach is that the dose to the patient need not be increased as a consequence of scatter removal. The disadvantage is a substantial increase in x-ray tube heat load.

At the current state of development, the cerium anode x-ray tube is limited to fluoroscopic techniques only. For conventional mammographic imaging, this might be adequate due to higher penetration of these photons. However, for contrast mammography the dual requirements of heavy filtration and scatter removal make the cerium anode tube inadequate for clinical imaging. New developments in anode construction and materials will be required to make it useful. The W/Ce system, however, has excellent promise as a tool for observing low-contrast iodine concentrations seen in work with the CT/M.

SUMMARY

Luminance scatter-to-primary ratios were measured for Mo/Mo, W/Ce, and Ce/Ce anode/filter combinations using a polyethylene phantom. The Mo/Mo S/P measurements were somewhat higher than previously reported values for Lucite phantoms. S/P values for the cerium-filtered spectra were substantially higher, making scatter removal more important for these spectra.

ACKNOWLEDGMENTS

This work has been supported in part by the National Science Foundation under NSF Grant No. ECS-7926658. Our gratitude is also expressed to T. Lesensky, Ph.D. of Machlett Laboratories, for constructing the cerium anode tube and offering significant support in its use, to Murray Cleare of Eastman Kodak for supplying the H&D reference data, and to Miss Theresa Stika for valuable assistance in preparing the manuscript.

APPENDIX: THE EFFECT OF S/P ON SIGNAL-TO-NOISE RATIO ON IMAGES MADE WITH A MONOENERGETIC X-RAY SOURCE

The fundamental limiting factor in radiographic SNR is photon fluence. For a radiographic image produced by a monoenergetic source, the fluence is given by

$$N_t = N_p + N_s, \tag{A1}$$

where N_t is the total photon fluence, N_p is the primary photon fluence, and N_s is the scattered photon fluence. Assuming that the signal seen against this background does not perturb the scattered photon fluence, then

$$N_t' = N_p' + N_s, \tag{A2}$$

where N_t' is the total photon fluence behind the target giving rise to the signal and N_p' is the primary photon fluence behind the target. Thus the observable signal Ω is given by

$$\begin{aligned}\Omega &= N_p' + N_s - N_p - N_s \\ &= N_p' - N_p = \Delta N_p.\end{aligned} \tag{A3}$$

Assuming Poisson statistics for the photon fluence, the noise in the target area is given by

$$\begin{aligned}\sigma^2 &= N_p + N_s \\ &= \left(1 + \frac{S}{P}\right)N_p.\end{aligned} \tag{A4}$$

Designating the "noise" as σ, then

$$\begin{aligned}\mathrm{SNR} &= \Omega/\sigma \\ &= \Delta N_p \Big/ \sqrt{\left(1 + \frac{S}{P}\right)N_p}.\end{aligned} \tag{A5}$$

In the absence of scatter,

$$\mathrm{SNR} = \Delta N_p/\sqrt{N_p}. \tag{A6}$$

Thus the SNR is reduced by scatter by the multiplicative factor $1/\sqrt{1+(S/P)}$. To restore the SNR to its value without scatter, N_p (and dose) must increase by $[1+(S/P)]$.

For subtraction systems, the situation is even worse. In a temporal subtraction system, two images which are identical save for the introduction of a small contrast change are combined to create a difference image with very low background

to improve the contrast and remove structured noise. The background in each of two such images is

$$N_{ti} = N_{pi} + N_{si}, \quad i = 1,2. \tag{A7}$$

The background fluence in the subtraction image is therefore

$$N_{t-} = (N_{p2} - N_{p1}) + (N_{s2} - N_{s1}). \tag{A8}$$

Similarly, the signal fluence in the subtracted image is

$$N'_t = (N'_{p2} - N'_{p1}) + (N_{s2} - N_{s1}) \tag{A9}$$

and the observable $\Omega -$ is

$$\begin{aligned}\Omega - &= (N'_{p2} - N_{p2}) - (N'_{p1} - N_{p1}) \\ &= \Omega_2 - \Omega_1.\end{aligned} \tag{A10}$$

The noise in the target area of the subtraction image is given by

$$\sigma^2_{\Omega -} = N_{P2} + N_{p1} + N_{s2} + N_{s1}. \tag{A11}$$

Assuming that $(S/P)_1 \cong (S/P)_2$, we have

$$\sigma^2_{\Omega -} = 2\left(1 + \frac{S}{P}\right)N_p. \tag{A12}$$

Thus the SNR of a subtraction image, compared to an unsubtracted image without scatter, is degraded by $1/\sqrt{2[1 + (S/P)]}$. Furthermore, if both Ω_1 and Ω_2 have the same sign, then $|\Omega - | \leqslant \Omega_j$, where j is the subscript of the image with highest presubtraction contrast. Thus to obtain SNR in the subtracted image equal to the SNR in the original image without scatter requires an increase in dose by at least a factor of $2[1 + (S/P)]$.

For polychromatic x-ray beams, it is the variance in energy absorbed which is of interest, not simply the number of photons. However, for quasi-monoenergetic spectra with small energy variance, the monoenergetic approximation is reasonable.

In the event that dose is not increased to compensate for scatter, then SNR decreases by the appropriate factor. For quantum limited detection problems, where a threshold SNR determines the minimum detectable contrast for a given object, the minimum detectable contrast increases with increasing scatter. For the single image case, the minimum detectable contrast rises as $\sqrt{1 + (S/P)}$. In the case of a subtraction image, the minimum detectable contrast rises with $\sqrt{2[1 + (S/P)]}$.

[1] C. H. J. Chang, J. L. Sibala, S. L. Fritz, S. J. Dwyer III, A. W. Templeton, F. Lin, and W. R. Jewell, Cancer 46, 939 (1980).
[2] F. Kelcz, C. A. Mistretta, and S. J. Riederer, Med. Phys. 4, 26 (1977).
[3] R. A. Kruger, S. J. Riederer, and C. A. Mistretta, Med. Phys. 4, 244 (1977).
[4] F. Kelcz and C. A. Mistretta, Med. Phys. 3, 159 (1976).
[5] J. Heinzerling and M. Schlindwein, IEEE Trans. Nucl. Sci. 27, 961 (1980).
[6] G. T. Barnes and I. A. Brezovich, Radiology 126, 243 (1978).
[7] G. T. Barnes, "Characteristics of Scatter," in *Reduced Dose Mammography*, edited by W. W. Logan and E. P. Muntz (Masson, New York, 1979).
[8] M. Friedreich, Fortsher. Geb. Roetgenstr. 123, 556 (1975).
[9] D. Gur, D. Sashin, and D. L. Herbert, "Improved Contrast in Mammography Using a Double Slit Technique," 25th Annual Meeting of the Association of University Radiologists, Kansas City, May, 1977.
[10] W. Hoeffken, G. Jotlen, and D. Richter, Medicamundi 22, 61 (1977).
[11] E. P. Muntz, "On the Significance of Scattered Radiation in Reduced Exposure Mammography," Paper No. 105 presented at the Annual Meeting of the Radiological Society of North America, Chicago, 1977.
[12] C. E. Dick and J. W. Motz, Med. Phys. 5, 133 (1978).
[13] W. Kalender, Phys. Med. Biol. 26, 835 (1981).
[14] C. E. Dick, C. G. Soares, and J. W. Motz, Phys. Med. Biol. 23, 1076 (1978).
[15] M. V. Yester, G. T. Barnes, and M. A. King, Med. Phys. 8, 158 (1981).

1006887

Critical Pathways for the Future: MR Imaging and Digital Mammography[1]

Gillian M. Newstead, MD • Jeffrey C. Weinreb, MD

■ INTRODUCTION

Breast MR imaging is one of the most promising and controversial areas in breast imaging today. The promise lies in the possibility that MR imaging may allow detection of mammographically occult cancers and play an important role in the evaluation of patients with postsurgical changes and in patients in whom mammography is of limited use, such as those with radiographically opaque breasts. MR imaging is generally accepted to be the most effective method of assessing the integrity of breast implants. Many physicians are skeptical about the usefulness of this technique and suggest that MR imaging may not provide cost-effective information that will ultimately affect patient treatment and outcome. There are some biologic and physical limitations that radiographic imaging of the breast is not likely to overcome. The introduction of intravenously administered gadolinium contrast agents, dedicated breast radiofrequency coils, and faster imaging techniques has significantly changed the diagnostic possibilities. Enhancement and morphologic characteristics may be used to differentiate benign and malignant lesions, and some investigators have stated that the absence of an abnormal finding on MR images is a reliable means of excluding carcinoma (1).

Many experts predict that the development of digital technology for breast imaging will result in significant improvement in mammography. The advantages of digital techniques include amplification of subject contrast and a wider dynamic range, allowing greater variation in exposure factors. Image processing techniques allow manipulation of images to enhance the conspicuity of subtle lesions. Research is currently directed toward the development of detectors for whole breast imaging and the design of display systems that meet the higher spatial requirements needed. Additional advantages include more efficient image storage and the ability to transmit images to remote sites. These systems must be cost-effective to achieve widespread clinical use. Computer-aided diagnosis—the use of digital technology to assist the radiologist—may perhaps prove useful in the future.

■ CONTRAST-ENHANCED MR IMAGING OF THE BREAST

• Techniques

Most invasive breast cancers enhance rapidly and profoundly after intravenous injection of gadolinium contrast agents, and this enhancement makes them conspicuous on MR images. These contrast agents are distributed in the extracellular space after intravenous injection and tend to accumulate in tissues with rich vascularity (2). The secretion of tumor angiogenesis factor promotes the recruitment of new blood vessels, resulting in the high vascularity of most breast cancers larger than 1 cm in diameter. Benign lesions are relatively poorly vascularized (3). Generally, breast cancers enhance more rapidly and profoundly after bolus injection of paramagnetic agents (4,5). Other factors likely accounting for the enhancement patterns of breast cancers include an increase in capillary permeability, changes in osmolar pressure, and expansion of the interstitial space (2,6).

There are many different techniques reported for the performance of breast MR imaging. No standard, universally recognized method exists, and the various techniques available are varied and complex. It is generally accepted that T1-weighted sequences performed before

Mammographie : MR / Digital M. ; Bewertung

Index terms: Breast, biopsy, 00.1261 • Breast, MR, 00.12143 • Breast neoplasms, diagnosis, 00.31, 00.32 • Breast, postoperative, 00.45 • Breast, prostheses, 00.4543 • Breast, radiography, 00.1215 • Computers, diagnostic aid • Gadolinium, 00.12143

RadioGraphics 1995; 15:951–962

[1] From the Department of Radiology, New York University Medical Center, 530 First Ave, New York, NY 10016. From the Critical Pathways in the Management of Breast Disease Plenary Session at the 1994 RSNA scientific assembly. Received March 27, 1995; revision requested April 13 and received May 26; accepted May 26. Address reprint requests to G.M.N.

Figure 1. Lobular carcinoma in a 43-year-old woman with a spiculated mass noted on a screening mammogram. (a) Spot magnification mammogram shows the lesion in the left breast. (b) Subtraction MR image (postinjection-preinjection data set) obtained to search for satellite lesions shows an irregular mass with rim enhancement, typical of carcinoma. There was no evidence of multifocal disease. (c) Enhancement curve (*x* axis = time, *y* axis = degree of enhancement) shows rapid intense enhancement, typical of a malignant lesion. An 8-mm-diameter invasive lobular carcinoma was found at histologic examination. Image range = 48, 112, 176, 240, 304, 368.

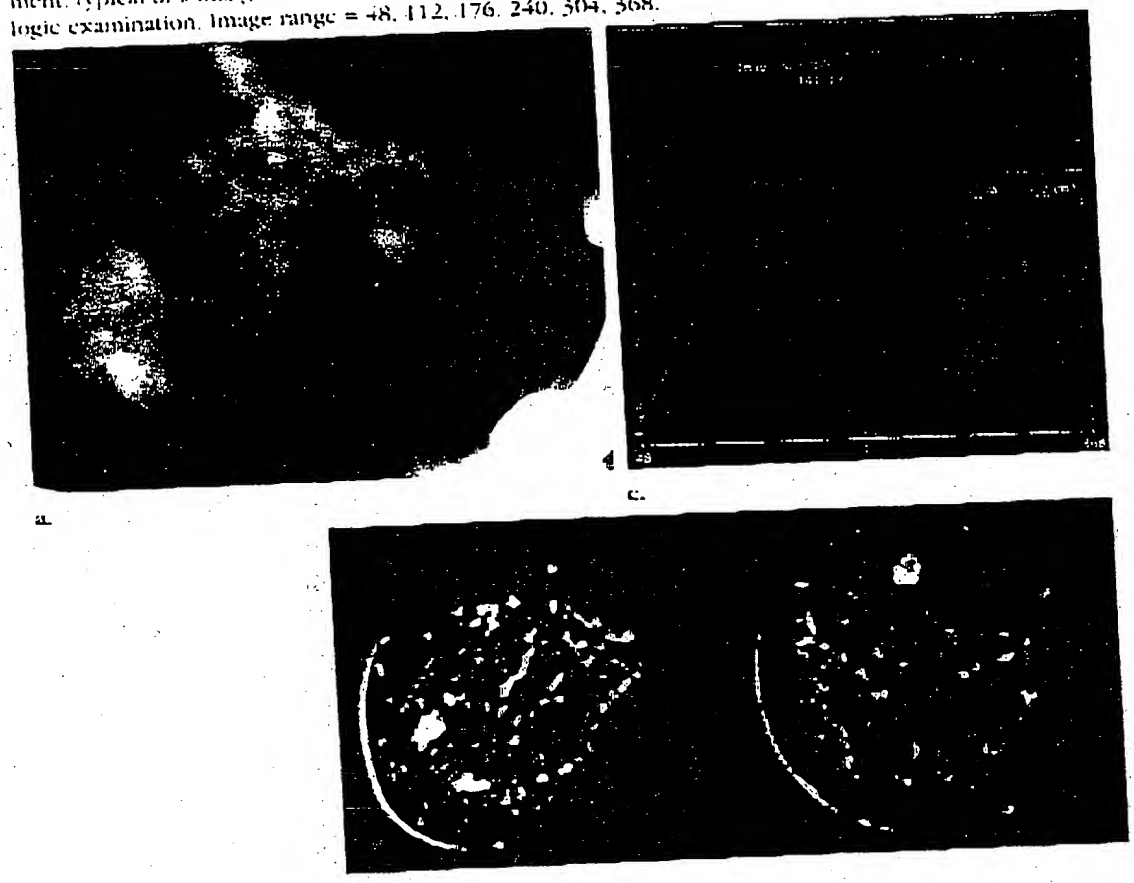

and after injection of gadolinium contrast agents are required to detect and characterize lesions. Various gradient-echo and spin-echo techniques have been used (7–10). High-resolution techniques together with rapid acquisition and fat suppression have been advocated by Harms et al (11). Two-dimensional imaging studies with excellent results have been reported; however, three-dimensional techniques are probably preferable, as they provide high signal-to-noise ratio, gapless, high-resolution images expeditiously. Multiplanar reformatted images allow excellent appreciation of spatial relationships (8). Most techniques aim to strike a balance between spatial and temporal resolution.

The breast imaging technique used for most breast examinations at our institution provides excellent image quality. Coronal images are obtained before injection, and image acquisition is repeated five times after administration of contrast material with an acquisition matrix of 96 × 256 (in-plane spatial resolution, 1.25 × 1.4 × 1.4 mm) by using a three-dimensional spoiled gradient-echo sequence (fast low-angle shot, repetition time of 14 seconds, echo time of 7 msec,

Figure 2. Fibroadenoma in a 35-year-old woman with multiple palpable lesions in the right breast. (a) Mammogram (90° lateral view) demonstrates dense breast tissue with multiple circumscribed masses. The dominant palpable mass is marked with a skin BB. (b) Unenhanced sagittal subtraction MR image demonstrates multiple lobulated masses. (c) Enhanced sagittal MR image shows multiple lobulated masses that enhance to varying degrees (arrows). Internal septations are present in the masses, typical of fibroadenoma. The four palpable lesions were shown to be fibroadenoma with fine-needle aspiration.

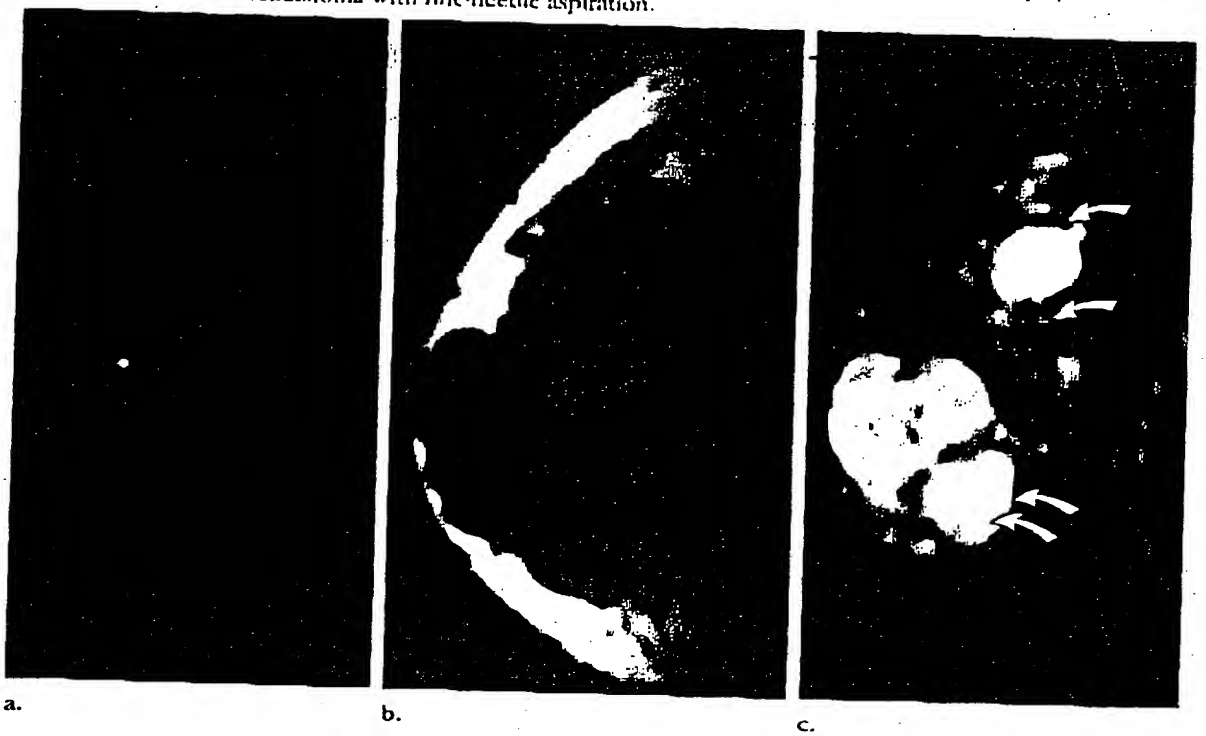

a. b. c.

flip angle of 25°, and one signal averaged). Each sequence produces a set of 64 2.5-mm-thick sections in less than 1.5 minutes, with a total imaging time of less than 10 minutes. Maximum-intensity projection can be performed on the subtracted data sets to distinguish enhancing lesions from blood vessels. Multiplanar reconstruction can also be performed on any of the data sets to produce three-dimensional images. Information about the rate and degree of enhancement of a lesion can be obtained by placing a region of interest on the area of concern and generating enhancement curves, which graph the signal intensity at six points in time.

• Characterization of Breast Lesions

It has been reported that breast cancers enhance consistently with gadolinium contrast agents (Fig 1) and that most benign lesions enhance slowly or not at all (4,12). In one series of 119 documented breast cancers (reported in a non–peer-reviewed publication), 100% showed at least 90% enhancement during the 1st minute, and maximum signal intensity was reached within 2 minutes. Enhancement then tended to plateau, with some cancers subsequently showing a slight increase or decrease. There is good evidence that breast carcinomas tend to enhance faster, and washout earlier, than benign tissues (10,12). The problem is that benign and precancerous tissues also enhance. These tissues include fibroadenoma (Fig 2), nonproliferative and proliferative fibrocystic changes (Fig 3), inflammatory change, fresh scar, sclerosing adenosis, lobular carcinoma in situ, and atypical ductal hyperplasia (4,11).

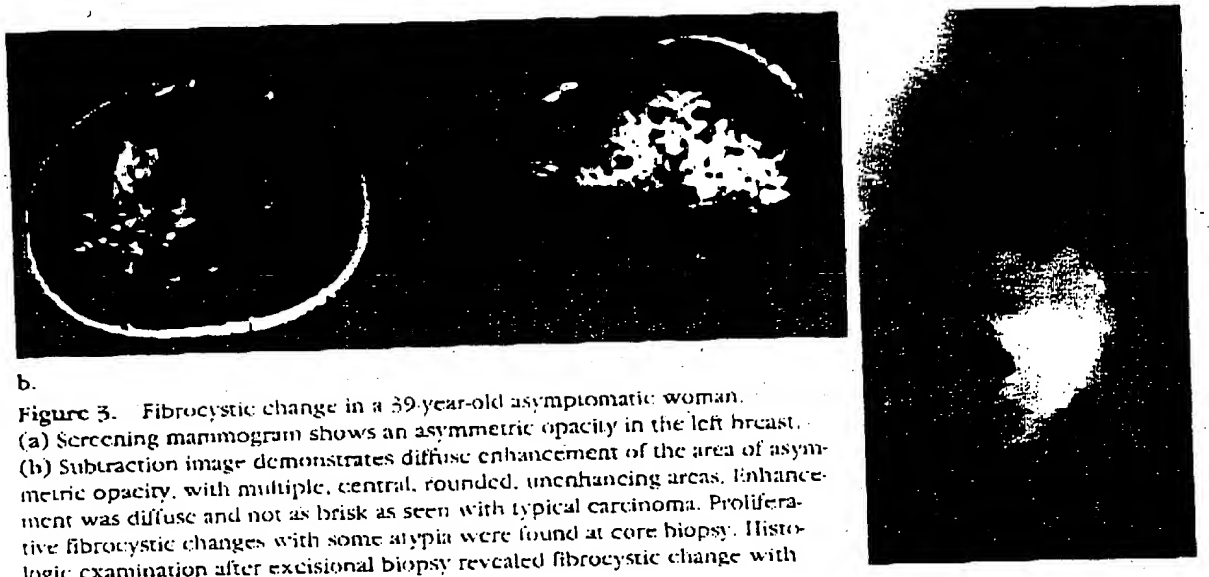

b.

a.

Figure 3. Fibrocystic change in a 39-year-old asymptomatic woman. (a) Screening mammogram shows an asymmetric opacity in the left breast. (b) Subtraction image demonstrates diffuse enhancement of the area of asymmetric opacity, with multiple, central, rounded, unenhancing areas. Enhancement was diffuse and not as brisk as seen with typical carcinoma. Proliferative fibrocystic changes with some atypia were found at core biopsy. Histologic examination after excisional biopsy revealed fibrocystic change with mild atypia.

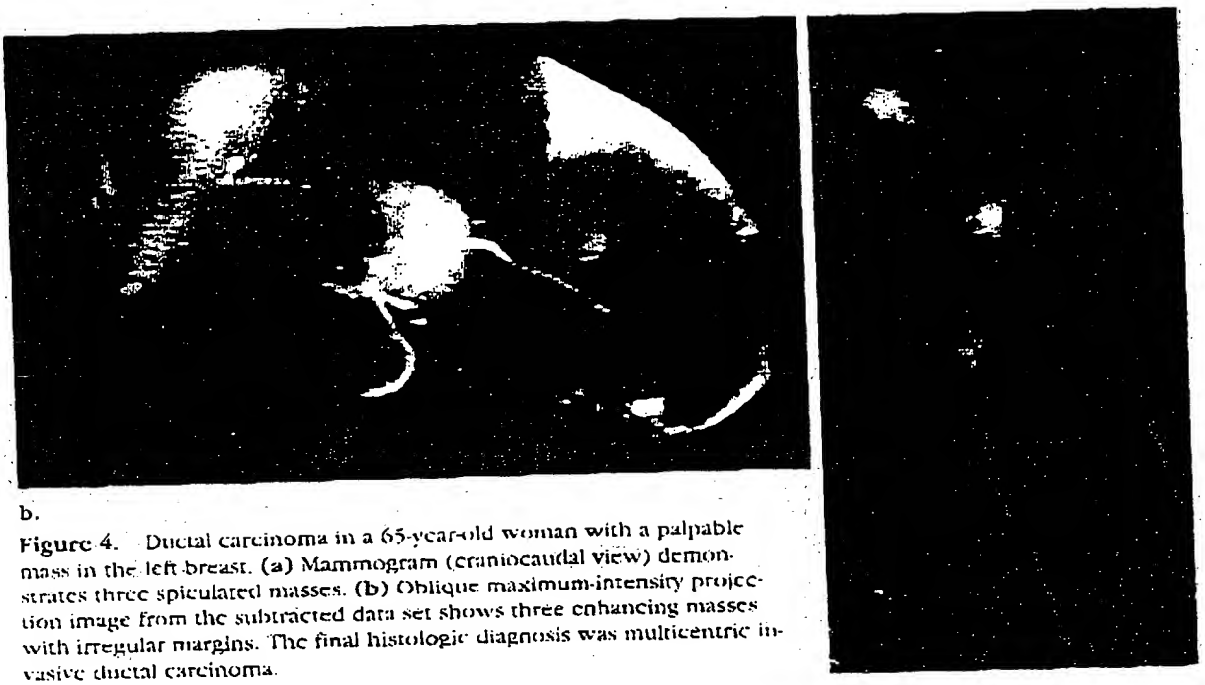

b.

a.

Figure 4. Ductal carcinoma in a 65-year-old woman with a palpable mass in the left breast. (a) Mammogram (craniocaudal view) demonstrates three spiculated masses. (b) Oblique maximum-intensity projection image from the subtracted data set shows three enhancing masses with irregular margins. The final histologic diagnosis was multicentric invasive ductal carcinoma.

It has also been shown that some cancers enhance slowly or not at all (10,13,14). A pattern of rim enhancement has been noted in cancers but not in benign tumors (10,15) (Fig 1b). A recent study (16) designed to use a temporal resolution of 2 seconds showed that benign lesions initially enhanced centrally but cancers enhanced from the periphery to the center. Most cancers exhibit irregular margins (Figs 4, 5), whereas benign lesions such as fibroadenoma often have smooth, lobulated borders with internal septations (13) (Fig 2c). If the lesion enhancement rate and pattern are considered, together with the lesion morphology, more precise discrimination will be possible.

• Assessment of the Preoperative Breast

Is it possible that MR imaging can enable more accurate assessment of the size, margins, number, and location of breast cancers and thus al-

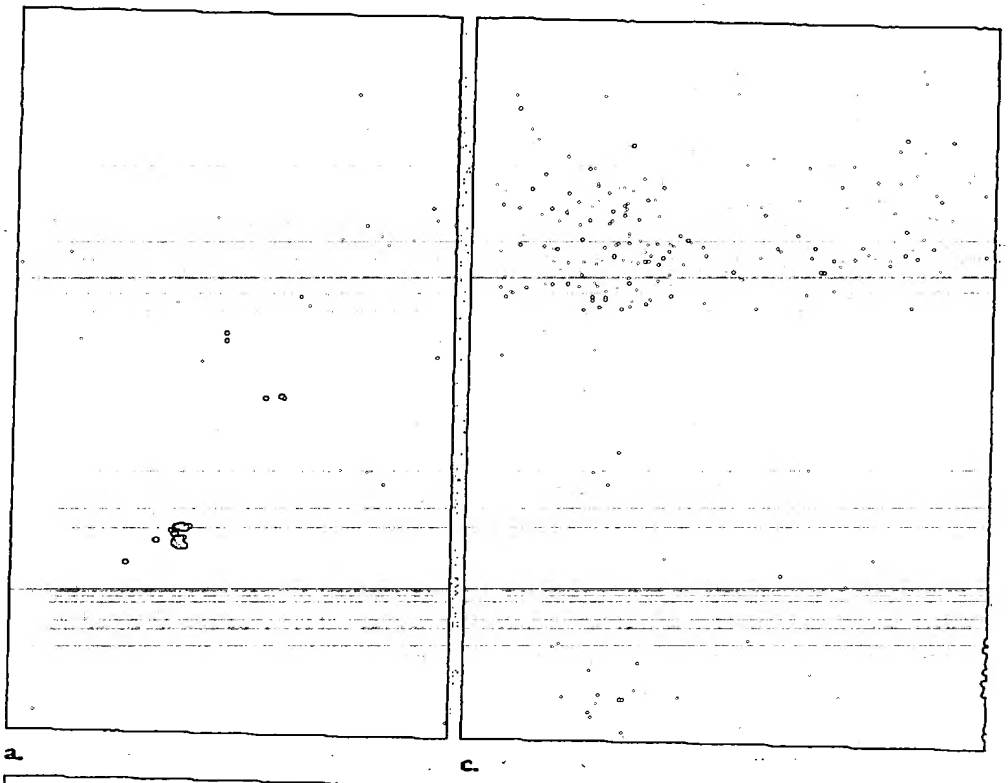

a.

c.

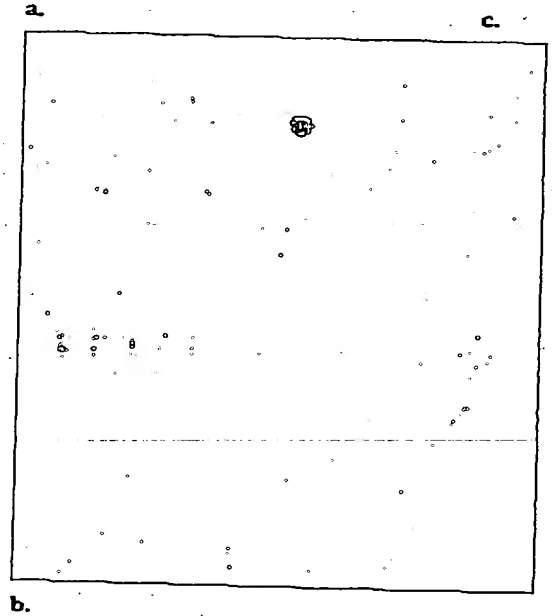

b.

Figure 5. Ductal carcinoma in a 60-year-old asymptomatic woman. (a) Screening mammogram (mediolateral oblique view) of the right breast demonstrates an ill-defined opacity with calcifications in the superior aspect of the breast. (b) Mammogram (spot magnification view in the craniocaudal projection) shows a BB marking the site of the skin lesion. (c) Sagittal subtraction gadolinium-enhanced MR image obtained as part of a research protocol shows irregular enhancement corresponding to the mammographic findings. Histologic examination revealed an 11-mm-diameter invasive ductal carcinoma with an extensive intraductal component (high nuclear grade).

low more accurate preoperative imaging evaluation? Multifocality and multicentricity of breast cancer is found with MR imaging in many patients with a unifocal mammographic lesion. Several investigators have shown that MR imaging is more sensitive in detecting additional lesions in these patients (8,17). It is postulated that this reported improvement in sensitivity compared with mammography may result in reassessment of treatment options and perhaps reduce the likelihood of tumor recurrence by providing the surgeon with a more accurate estimation of tumor extent. In one study (18) of 18 such patients with breast cancer, the results of MR imaging caused the planned treatment to be changed in nine cases because of new information about size, multifocality, multicentricity, and chest wall invasion. However, unless reli-

able criteria are developed to distinguish between benign and malignant enhancing lesions, use of MR imaging evaluation could result in inappropriate therapy.

MR imaging may be useful for evaluation of patients with axillary nodes positive for adenocarcinoma and normal mammographic and ultrasound (US) findings (17,18). Identification of the primary lesion might allow more limited surgery and provide important histologic information for therapy planning. MR imaging is also useful in assessing patients treated with preoperative chemotherapy. Pre- and posttreatment images are compared to determine response to treatment more accurately (19).

• Assessment of the Posttreatment Breast

Early detection of local recurrence improves long-term survival, but mammographic evaluation of these patients is often difficult. Prominent enhancement of nonneoplastic tissues up to 9 months after therapy has been reported; however, from 9 to 18 months after treatment, MR imaging can be used to detect or exclude recurrent tumor. In one series, there was no significant enhancement after 18 months in 30 of 32 cases, whereas diffuse enhancement was noted in all recurrent tumor (20,21). These initial encouraging results suggest that MR imaging will likely become an important adjunctive diagnostic method for evaluation of the posttreatment breast.

• Evaluation of Breast Prostheses

Evaluation of the integrity of breast implants accounts for a large percentage of breast MR imaging examinations. The complications of silicone gel implants include capsular fibrosis, calcification, and contraction with subsequent hardening and cosmetic deformity. Silicone can migrate through the outer envelope of the implant via a frank rupture or bleed through an intact envelope. Free silicone can enter the surrounding breast tissue and migrate via lymphatics to local lymph nodes or to distant parts of the body (22). Immune-related diseases have been reported to be associated with the presence of free silicone in some patients (23).

More than 1 million American women have undergone breast augmentation procedures, with a variety of silic ne implants placed in the breast for cosmetic or reconstructive purposes (24). These implants are usually single lumen or double lumen (in which the silicone shell is usually surrounded by a saline bag) and consist of an envelope of Silastic elastomer (Dow Corning, Midland, Mich) filled with silicone gel. They are placed in either a retroglandular or subpectoral location. MR imaging is uniquely suited to image silicone and silicone implants, and reports suggest that MR imaging may allow the most accurate assessment of implant status.

There are multiple possible approaches to MR imaging of silicone, and these depend to some extent on the equipment and sequences available. At our institution, we currently perform a number of different complementary sequences and achieve reliable images for the thorough assessment of implants. The patient is imaged in the prone position with a bilateral receive-only dedicated breast coil. A scout sagittal image is obtained, followed by performance of an axial T2-weighted hybrid rapid acquisition with relaxation enhancement (RARE) (ie, turbo spin-echo) sequence through both breasts and the axilla (repetition time of 5,000 msec, echo time of 180 msec, 5-mm section thickness, 190 × 512 matrix, 350-cm field of view). The final sequence performed is a frequency-selective water-suppressed T2-weighted hybrid RARE sequence in which silicone and fat have high signal intensity.

Normal implants have smooth, well-defined margins, and surface radial folds are often visible. Double-lumen implants are easily identified. Knowledge of the type of implant is helpful in image interpretation. An intact single-lumen implant may mimic a double-lumen implant with a collapsed outer saline envelope. An intracapsular rupture is defined as an envelope rupture with pieces of free-floating silicone shell noted within the gel contained by the fibrous capsule. This has been called the "linguine sign," with multiple curvilinear structures noted within the silicone on MR images (25) (Fig 6). Another sign of intracapsular rupture is the "water droplet sign" or "salad oil sign," with multiple droplets of fluid of extracapsular origin or from a surrounding saline envelope noted within the silicone implant lumen (26). Extracapsular rupture is defined as leakage of silicone beyond the confines of the fibrous capsule. Such rupture is seen easily on MR images and often also on mammograms and

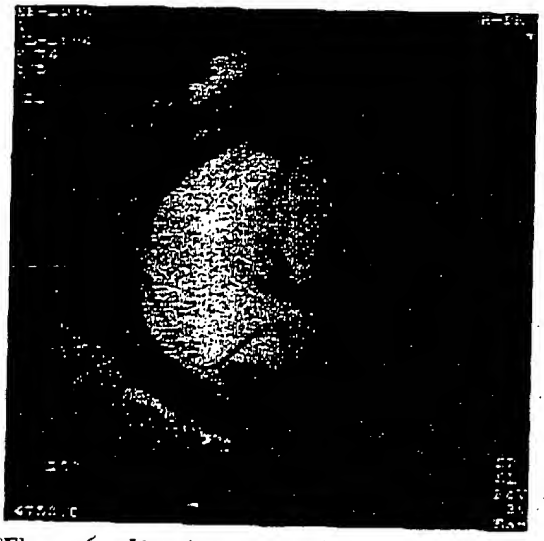

Figure 6. Linguine sign in a 56-year-old woman with retroglandular silicone implants placed 15 years ago. Sagittal T2-weighted spin-echo MR image (repetition time msec/echo time msec = 4,750/120) obtained for assessment of implant status shows evidence of an intracapsular rupture, with pieces of the implant shell floating within the silicone.

US scans. Irregular implant contour, adjacent fluid collections, or bulges are unreliable signs of rupture (26).

• MR Imaging–guided Biopsy

Use of MR imaging–guided needle biopsy systems may be necessary, particularly when a suspicious lesion is visible only on MR images. Several systems have been developed, most of which employ a unilateral radio-frequency coil with perforated compression plates. The breast is imaged, and the coordinates of the lesion are determined from the images. The needle is then inserted through the appropriate aperture, and the patient is reimaged to confirm accurate needle placement. The current systems under study appear to be adequate for placement of a wire for localization before surgical excision in most cases. Further refinements appear to be necessary for reliable performance of MR imaging–guided fine-needle aspiration or core needle biopsy. Computer-driven needle-guidance systems and a full range of nonferromagnetic needles and biopsy guns are not yet available.

• The Future

At this time, and for most applications, breast MR imaging is in the investigational stage. The advantages of this technique include the absence of ionizing radiation and the detection of mammographically occult lesions. MR imaging examinations of the breast are currently performed with a wide variety of techniques, coils, and field strengths. Imaging protocols, postprocessing techniques, and biopsy systems are being evaluated. The cost-effectiveness of MR imaging must also be studied, and a cost-benefit analysis will be needed before breast MR imaging examinations become uniformly reimbursable.

A controlled study with careful comparison of conventional breast imaging, MR imaging, and pathologic correlation has not yet been completed, to our knowledge. Further research may lead to a better understanding of breast pathophysiology and perhaps ultimately provide an improved method for the detection, characterization, and possibly treatment of breast cancer.

■ DIGITAL MAMMOGRAPHY

• Limitations of Screen-Film Mammography

Conventional screen-film mammography is currently the most effective method for detection of small breast cancers. Use of mammographic screening has shown that the absolute mortality from breast cancer can be reduced by 30% (27). Significant improvements have been made in mammographic technology since the early development of mammographic techniques, such as those reported by Egan (28). Screen-film mammography has greater sensitivity and specificity for detection of breast cancer than any other diagnostic technique available today. The development of improved tube designs with small focal spots and improved screen-film combinations, grids, and film processing has resulted in better image quality and lower patient dose (29).

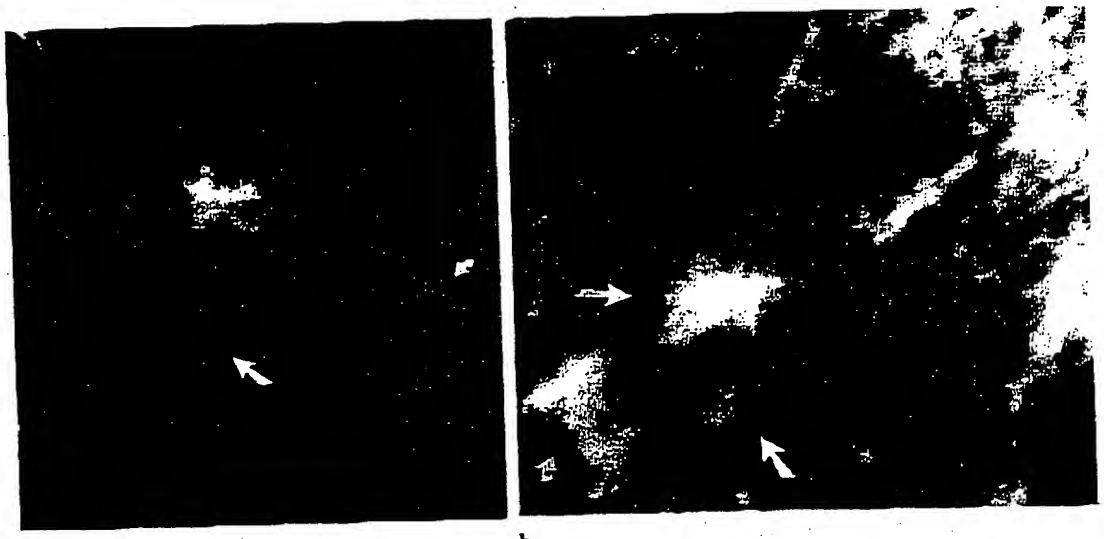

a. b.

Figure 7. Use of increased contrast sensitivity in a 68-year-old woman with a palpable mass in the inferior aspect of the left breast. **(a)** Mammogram (spot magnification view) shows a multifocal spiculated carcinoma. Two satellite spiculated masses (arrows) are noted adjacent to the primary lesion. **(b)** Digital mammogram (spot view) obtained in the prone position with different obliquity and with contrast enhancement image processing shows the spiculated masses (arrows).

Mammographic film techniques provide good spatial resolution and high-contrast images of tissues with inherently low contrast. The film functions both as the image acquisition detector and the display and storage mechanism. The major technical limitations involve compromises in image contrast and latitude, as well as film granularity (30,31). High-contrast images are essential for detection of small cancers because the x-ray attenuation properties of benign and malignant tissues are very similar (32). Film has a nonlinear response to light emitted from a phosphor screen, and a limited range of optical densities can thus be displayed. The detection of all types of breast lesions is limited by inherent film noise. Film granularity is a major source of noisy images; to overcome this problem, an increased radiation dose is often needed (33).

• Advantages of Digital Mammography

Digital mammography has many potential advantages over conventional screen-film techniques, especially in terms of image display, processing speed, and image transmission (34,35). Digital systems acquire, display, and store the images independently; therefore, each of these functions can be optimized individually. Manipulation of images with interactive windowing and filtration can enhance certain structures and improve lesion conspicuity. The major considerations for the design of a digital mammography system are contrast sensitivity and spatial resolution. The limiting spatial resolution of most screen-film systems is approximately 20 line pairs per millimeter (lp/mm). However, there is evidence that, despite the lower spatial resolution of digital systems (typically < 10 lp/mm), lesion conspicuity can be improved by means of increased contrast sensitivity (30) (Fig 7).

• Small-Field Detectors

Digital mammographic systems with a small field of view are used widely today for stereotaxic breast biopsy. These systems use a charge-coupled device image sensor that is coupled to an x-ray intensifying screen with either a fiberoptic cable or a lens. A phosphor screen is used to convert the images to light in both types of systems. The image produced is then recorded by a charge-coupled device camera rather than by film. These systems have a small field of view (5 cm) and adequate spatial resolution (10

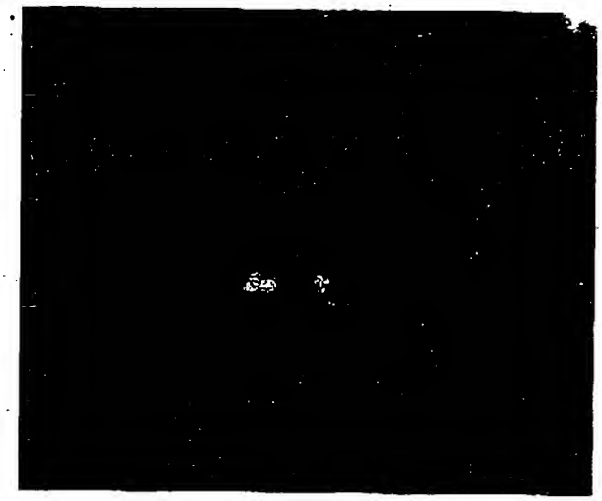

a.

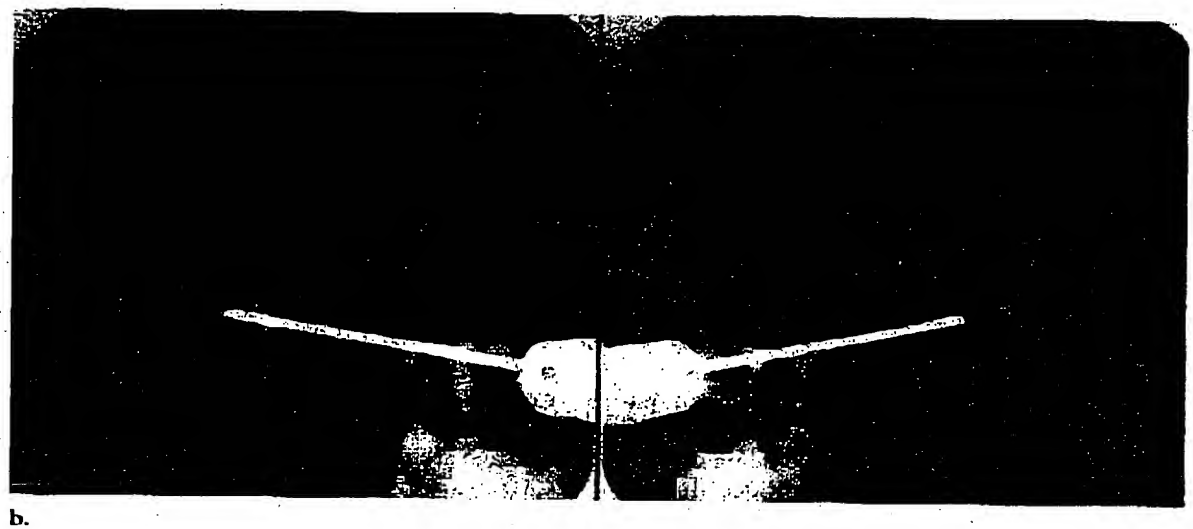

b.

Figure 8. Use of a small-field detector in a 52-year-old woman with a 13-mm-diameter lobulated nodule detected on a screening mammogram. (a) Coned compression magnified digital mammogram obtained in the prone position before stereotaxic biopsy shows a lesion. (b) Stereotaxic mammograms obtained during fine-needle aspiration show the needle placed centrally in the lesion.

lp/mm). Manufacturers of such systems include LoRad Medical Systems (Danbury, Conn) and Fischer Imaging (Denver, Colo). The digital capability greatly decreases procedure time, and the ability to enhance the images improves lesion conspicuity (Fig 8).

• Full-Field Detectors

Ongoing research is now directed to the development of full-field digital mammographic systems. The main focus of these efforts involves detector design. The requirements include efficient absorption of and a linear response to the incident radiation beam. Adequate spatial resolution (10 lp/mm) and an 18 × 24-cm field of view are necessary. An acceptable imaging time is also a significant consideration. Demagnification camera systems provide a method of obtaining a full-field digital mammogram by coupling a large-area phosphor to a small-area photodetector (charge-coupled device) via a lens or fiberoptic cable. The principal problem with these systems is inefficient optical coupling, causing unacceptable signal and noise characteristics (36).

Figure 9. Comparison of conventional mammogram (left) and full field digital mammogram (right) (cranio caudal views).

Another approach under consideration involves use of photostimulable phosphors. Electrons in the phosphor are excited by the x-ray beam, captured, and stored in traps in the phosphor crystals. An image is produced by scanning the phosphor plate with a focused laser beam. This system currently lacks adequate spatial resolution for mammography (37). Amorphous selenium detectors are also being developed. Selenium can be used to produce an electrostatic image with high resolution. The digital image is acquired by scanning a laser beam over the selenium plate (38). Large-area detectors that use amorphous silicon are also under investigation and may ultimately provide suitable digital images.

Alternative methods to use of large-area detectors to produce full-field digital mammograms are under investigation. A small-area detector, together with the radiation beam, is scanned across the breast to build a full image. The advantage of these systems is that the current digital technology, with an adequate spatial resolution, signal-to-noise ratio, and dynamic range, can be used to build the image (Fig 9). However, sequential image acquisition increases the exposure time. Scattered radiation at the image receptor is less of a problem than with full-area detector systems because only a fraction of the breast is irradiated at any time (39).

• Computer-aided Diagnosis

Computer-aided diagnosis (CAD) is an intriguing concept. Investigators at the University of Chicago are exploring the possibility of using CAD to identify lesions missed by human observers. CAD is designed to alert radiologists to the site of a possible lesion. Studies have shown that the diagnostic accuracy of image interpretation by radiologists can be improved with the aid of computerized analysis techniques. The aims of CAD are to improve the sensitivity of mammography by increasing the detection of significant lesions (40). Computers can scan an image consistently, and the computer analysis could be used by the radiologist as a "second reading." CAD is in the development phase, and widespread use is not likely to occur until whole-breast direct digital mammographic systems are available.

• The Future

It seems likely that full-field digital mammographic systems will ultimately be developed. The ability to archive, retrieve, and display high-quality mammograms with a digital system

offers enormous benefits for improving practice efficiency. Remote transmission of these images would allow off-site interpretative and consultative services. Further research is needed to determine whether digital mammography and related technology will improve breast cancer detection in the future.

REFERENCES

1. Kaiser WA. MR mammography (MRM). Medica Mundi 1991; 36:168–182.
2. Strich G, Hagan PL, Gerber KH, Slutsky RA. Tissue distribution and magnetic resonance spin lattice relaxation effects of gadolinium-DTPA. Radiology 1985; 154:723–726.
3. Kaiser WA, Zeitler E. MR imaging of the breast: fast imaging sequences with and without Gd-DTPA (preliminary observations). Radiology 1989; 170:681–686.
4. Heywang SH, Wolf A, Pruss E, Hilbertz T, Eiermann W, Permanetter W. MR imaging of the breast with Gd-DTPA: use and limitations. Radiology 1989; 171:95–103.
5. Stack JP, Redmond OM, Codd MB, Dervan PA, Ennis JT. Breast disease: tissue characterization with Gd-DTPA enhancement profiles. Radiology 1990; 174:491–494.
6. Guillino PM, Grantham FH, Smith SW. The interstitial water space of tumors. Cancer Res 1965; 25:727–731.
7. Heywang SH, Hilbertz T, Beck R, Bauer WM, Eiermann W, Permanetter W. Gd-DTPA enhanced MR imaging of the breast in patients with postoperative scarring and silicone implants. J Comput Assist Tomogr 1990; 14: 348–356.
8. Harms SE, Flamig DP, Hesley KL, et al. MR imaging of the breast with rotating delivery of excitation off resonance: clinical experience with pathologic correlation. Radiology 1993; 187: 493–501.
9. Schnall MD, Orel S, Muenz L. Analysis of time intensity curves for enhancing breast lesions (abstr). In: Proceedings of the Society of Magnetic Resonance in Medicine 1993. Berkeley, Calif: Society of Magnetic Resonance in Medicine, 1993; 120.
10. Orel SB, Schnall MD, LiVolsi VA, Troupin RH. Suspicious breast lesions: MR imaging with radiologic-pathologic correlation. Radiology 1994; 190:485–493.
11. Harms SE, Flamig DP, Hesley KL, Evans WP. Magnetic resonance imaging of the breast. Magn Reson Q 1992; 8:139–155.
12. Kelcz F, Santyr GE, Mongin SJ, Fairbanks EJ. Reducing false positive gadolinium-enhanced breast MRI results through parameter analysis of the enhancement profile (abstr). In: Proceedings of the Society of Magnetic Resonance in Medicine 1993. Berkeley, Calif: Society of Magnetic Resonance in Medicine, 1993; 121.
13. Boetes C, Mus RD, Barentsz JO, Hendriks JH, Holland R, Rijs JH. Characterization of suspect breast lesions by using a gadolinium-enhanced dynamic TurboFLASH subtraction technique (abstr). Radiology 1993; 189(P):301.
14. Kaiser WA, Reiser M. False-positive cases in dynamic MR mammography (abstr). Radiology 1992; 185(P):245.
15. Rubens D, Totterman S, Chacko AK, et al. Gadopentetate dimeglumine–enhanced chemical-shift MR imaging of the breast. AJR 1991; 157:267–270.
16. Mus RD, Boetes C, Barentsz JO, Hendriks JH, Holland R, Ruijs JH. Combination of gadolinium-enhanced subtracted dynamic TurboFLASH and 3D MPRAGE sequences in the diagnosis of breast cancer (abstr). Radiology 1993; 189(P): 105.
17. Whitney WS, Herfkens RJ, Silverman J, Ikeda D, Brumbaugh J, Jeffrey S. Gadolinium-enhanced spectral-spatial MR imaging for evaluation of breast carcinoma (abstr). Radiology 1993; 189(P):136.
18. Deutch BM, Merchant TE, Schwartz LH, Powell CM, Liberman L, Dershaw DD. Local staging of breast cancer by using MR imaging (abstr). Radiology 1993; 189(P):301.
19. Segel M, Paulus D, Hortobagyi G. Advanced primary breast cancer: assessment at mammography of response to induction chemotherapy. Radiology 1988; 169:49–54.
20. Heywang-Koebrunner SH, Schlegel A, Beck R, et al. Contrast-enhanced MRI of the breast after limited surgery and radiation therapy. J Comput Assist Tomogr 1993; 17:891–900.
21. Dao TH, Rahmouni A, Campana F, Laurent M, Asselin B, Fourquet A. Tumor recurrence versus fibrosis in the irradiated breast: differentiation with dynamic gadolinium-enhanced MR imaging. Radiology 1993; 187:751–755.
22. Garrido L, Pfleiderer B, Papisov M, Ackerman JL. In vivo degradation of silicones. Magn Reson Med 1993; 29:839–843.
23. Steinbach BG, Hardt NS, Asbitt PL, Caffee HH. Breast implants, common complications, and concurrent breast disease. RadioGraphics 1993; 13:95–118.
24. Food and Drug Administration Bulletin: background information on the possible health risks of silicone breast implants (rev. February 8, 1991). Rockville, Md: U.S. Department of Health and Human Services, 1991.

25. Gorczyca DP, Sinha S, Ahn CY, et al. Silicone breast implants in vivo: MR imaging. Radiology 1992; 185:407–410.
26. Berg WA, Caskey CI, Hamper UM, et al. Diagnosing breast implant rupture with MR imaging, US, and mammography. RadioGraphics 1993; 13:1323–1336.
27. Tabar L, Fagerberg CJG, Gad A, et al. Reduction in mortality from breast cancer after mass screening with mammography. Lancet 1985; 1:829–832.
28. Egan R. Experience with mammography in a tumor institution: evaluation of 1000 cases. AJR 1960; 75:894–900.
29. Kimme-Smith C. New and future developments in screen-film mammography equipment and techniques. Radiol Clin North Am 1992; 30:55– 66.
30. Nishikawa RM, Mawdsley GE, Fenster A, Yaffe MJ. Scanned-projection digital mammography. Med Phys 1987; 14:717–727.
31. Vyborny CJ, Schmidt RA. Technical image quality and the visibility of mammographic detail. In: Haus AG, Yaffe MJ, eds. Syllabus: a categorical course in physics—technical aspects of breast imaging. Oak Brook, Ill: Radiological Society of North America, 1993; 103–111.
32. Johns PC, Yaffe MJ. X-ray characterisation of normal and neoplastic breast tissues. Phys Med Biol 1987; 32:675–695.
33. Barnes GT, Chakrabarty DP. Radiographic mottle and patient exposure in mammography. Radiology 1982; 145:815–821.
34. Templeton AW, Dwyer SJ, Cox GG, Johnson JA, et al. Picture archiving and communication systems (PACS) for radiology. In: Proceedings of CAR. Quebec, Canada: Canadian Association of Radiologists, 1985; 697–715.
35. McMillan JH, Huang HKB, Bramble JM, Siegel EL. Digital radiography. Invest Radiol 1989; 24:735–741.
36. Karellas A, Harris LJ, D'Orsi CJ. Small-field digital mammography with a 2,048 × 2,048 pixel charge-coupled device (abstr). Radiology 1990; 177(P):288.
37. Kato H. Photostimulable phosphor radiography design considerations. In: Seibert JA, Barnes GT, Gould RG, eds. Specification, acceptance testing and quality control of diagnostic x-ray imaging equipment: proceedings of the 1991 summer school. New York, NY: American Association of Physicists in Medicine, 1991.
38. Street RA. Hydrogenated amorphous silicon. Cambridge, England: Cambridge University Press, 1991; 391.
39. Holdsworth DW, Nishikawa RM, Mawdsley GE, Yaffe MJ, Fenster A. Slot-beam digital mammography using a time-delay integration (TDI) CCD. Proc SPIE 1989; 1090:306–313.
40. Schmidt RA, Nishikawa RM. Principles and practice of oncology. Vol 8, no. 7; 1–16.